ISSN 0036-0244, Russian Journal of Physical Chemistry A, 2021, Vol. 95, No. 3, pp. 523–529. © Pleiades Publishing, Ltd., 2021.
Russian Text © The Author(s), 2021, published in Zhurnal Fizicheskoi Khimii, 2021, Vol. 95, No. 3, pp. 426–433.

## IN COMMEMORATION OF ACADEMICIAN V.V. LUNIN: SELECTED CONTRIBUTIONS FROM HIS STUDENTS AND COLLEAGUES

# Surface Structure of Pt–Ni–Cr/C Catalysts

**T. V. Bogdan[a,b,*], A. N. Kalenchuk[a,b], S. V. Maksimov[a], and V. I. Bogdan[b,a]**

[a] *Department of Chemistry, Moscow State University, Moscow, 119991 Russia*

[b] *Zelinsky Institute of Organic Chemistry, Russian Academy of Sciences, Moscow, 119334 Russia*

**e-mail: chemist2014@yandex.ru*

Received September 2, 2020; revised September 2, 2020; accepted September 14, 2020

**Abstract**—The composition and structure of the surface phases of catalysts based on Pt, Ni, and Cr (platinum, bi- and trimetallic) supported on a Sibunit carrier are studied via TEM and EDS. The structure of the catalysts before and after reductive hydrogenation are compared. It is found that the metal in the Pt/C system is in a highly dispersed state, mainly in an oxidized form. In bimetallic and ternary catalysts, the surface contains metallic and oxide components; on the surface of Pt–Ni catalyst, the metal phase is more pronounced than with Ni–Cr and Pt–Ni–Cr. Nickel-based catalysts contain large metal particles (up to 30 nm). After reductive hydrogenation, an increase in dispersion and a reduction in the crystallinity of metal particles is observed in all of the studied systems.

*Keywords:* catalysts Pt/C, (Pt–Ni)/C, (Pt–Cr)/C, (Ni–Cr)/C, (Pt–Ni–Cr)/C, Sibunit, surface structure, TEM, EDS

**DOI:** 10.1134/S0036024421030067

## INTRODUCTION

Developing effective new catalysts for the hydrogenation of unsaturated organic compounds is of great practical and scientific interest. Heterogeneous catalytic reactions of hydrogenation-dehydrogenation, hydrogenolysis of C–C and C–O bonds, and natural gas reforming are usually conducted on catalysts based on noble and transition metals (e.g., Rh, Ru, Pt, Pd, and Ni) [1–3]. The electronic features of supported Pt-containing catalytic systems were considered in [4–13] in the context of their influence on catalytic activity. The dehydrogenation of cycloalkanes proceeds most effectively on Pt catalysts, but the need to reduce the content of the noble metal drives the search for alternative catalytic systems [5, 6] that combine Pt with transitional *d*-metals in particular [7, 8]. The interaction between the electron shells of Pt and transition metals reduces the electron density on the 5*d*-orbitals of Pt, improving the adsorption of reacting molecules on the catalyst surface [9]. In [10], a synergistic effect with respect to Pt/C during cyclohexane dehydrogenation was achieved on a PtNi/C-catalyst. In [11], the promoting effect Cr(III) has on Ni in binary NiCr systems was demonstrated in the reaction of methane reforming. The authors of [12] associated the effect of Cr(III) with the formation of crystallites that had the spinel structure of $NiCr_2O_4$ in NiCr systems. The increase in activity was presumably due to a greater surface area and the partial fusion of Ni and Cr, contributing to greater participation of Pt in the reaction than with binary catalysts [13]. The presence of complex multiphase alloys with Ni crystallites was noted in a three-component Pt–Ni–Cr catalytic system, but the X-ray diffraction patterns had none of the superstructure peaks at small angles that are characteristic of the formation of ordered intermetallic compounds. Weak reflections characteristic of chromium oxide were found.

Detailed study of the surface structure of catalysts is thus important for detecting active phases. In this work, transmission electron microscopy (TEM) and energy dispersive X-ray spectroscopy (EDS) were used to study the composition and structure of the surface phases of Pt–Ni–Cr deposited on a carbon support for catalysts with a reduced content of the noble metal and differing in the concentration of metals and the order of their deposition. The samples were examined when freshly prepared and after reductive activation with hydrogen.

## EXPERIMENTAL

### *Catalyst Preparation*

Metal catalysts were supported on a carbon support consisting of oxidized Sibunit ($C/Sib_{ox}$, Omsk) with an average granule diameter of 1.5–1.8 mm, a specific surface of 243 $cm^2/g$, an average pore size of 4.2 nm, and a volume of 0.45 $cm^3/g$ [13]. Monometallic catalysts Pt/C with Pt contents of 0.1 and 3 wt % were prepared by incipient wetness impregnation with a calculated amount of an aqueous solution of chloroplatinic

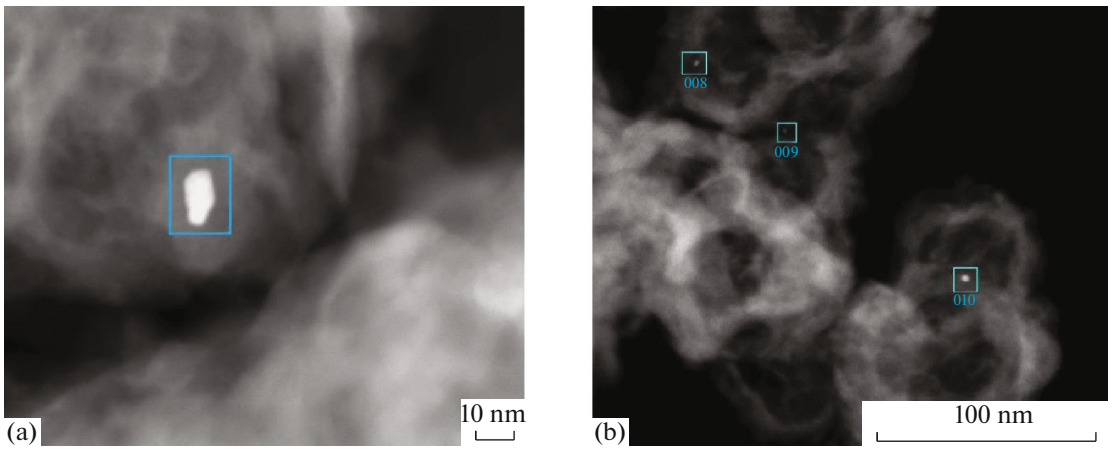


**Fig. 1.** Metal particles in a 0.1Pt/C sample and its EDS data: (a) particle with a linear size of 10 nm; (b) particles with linear sizes of 1–2 and 5 nm.

acid $H_2PtCl_6 \cdot 6H_2O$. Bimetallic systems with platinum were prepared by impregnating monometallic Ni/C and Cr/C systems obtained by impregnating the support with calculated amounts of an aqueous solution of $Ni(NO_3)_2 \cdot 6H_2O$ or $Cr(NO_3)_3 \cdot 9H_2O$, respectively. Three-component catalysts were obtained by applying an aqueous solution of $H_2PtCl_6 \cdot 6H_2O$ onto thermally treated nickel–chromium catalysts. Nickel–chromium catalysts on Sibunit support were prepared in two ways: (1) 3Ni/1.5Cr/C and 1.5Cr/3Ni/C catalysts were obtained by impregnating Cr/C and Ni/C samples, respectively; (2) (3Ni–1.5Cr)/C systems were prepared by co-impregnating the support with a mixtures of calculated amounts of aqueous solutions of nickel and chromium nitrates. Details on preparing catalysts and reductive hydrogenation experiments were described in [13]. The surface structure of original systems 0.1Pt/C, 3Pt/C, 0.1Pt/3Ni/C, (3Ni–1.5Cr)/C, and 0.1Pt/1.5Cr/3Ni/C was studied after preparation; that of systems 0.1Pt/3Ni/C, 0.1Pt/1.5Cr/C, and 0.1Pt/(3Ni–1.5Cr)/C and 0.1Pt/1.5Cr/3Ni/C, after reductive activation of the initial samples in hydrogen.

### *Studying the Structure of the Surface Phases of Catalysts*

The composition and surface structure of the catalysts were studied via transmission electron microscopy (TEM) on a JEOL-2100F (Japan) electron microscope in bright and dark field modes at an accelerating voltage of 200 kV. Elemental analysis of individual fragments was also performed via energy dispersive X-ray spectroscopy (EDS). Diffraction patterns were obtained for crystallites, the phase composition of which was determined by comparing EDS data and interplanar distances found from the diffraction patterns to reference values for pure metals and their alloys, oxides, and carbides, taken from an open database [14]. Some of the interplanar distances on whose basis the surface phases were identified, are given in Table 1. Particle size was estimated visually from TEM micrographs.

## RESULTS AND DISCUSSION

### *Structure of Unreduced Catalysts*

TEM of 0.1Pt/C catalyst samples allowed us to distinguish metal particles ranging in size from 1–2 to 10 nm (Figs. 1, 2). Due to the high dispersion of the deposited platinum and its low concentrations, we were unable to obtain diffraction patterns from the samples. The elemental composition of the regions containing metal particles testified to the presence of oxygen.

The EDS data show that carbon, oxygen, chlorine, and platinum atoms were present in samples of monometallic 3Pt/C catalyst. The presence of chlorine shows the incomplete removal of the initial salts during the calcination of the catalyst. The micrographs of the 3Pt/C samples show signs of the formation of a crystalline phase on the support (Fig. 3), for which we were able to obtain a diffraction pattern and estimate the characteristic interplanar distance: 0.393 nm. This value is close to the 0.392 nm for the (100) plane of metallic platinum (space group $Fm\bar{3}m$, $Z = 4$) and 0.395 nm for the (011) plane of mixed platinum oxide $Pt_3O_4$ (space group $Pm\bar{3}n$, $Z = 2$). Comparing these data, we may conclude there were oxidized platinum atoms on the surfaces of the carriers.

In the 0.1Pt/3Ni/C system, the characteristic size of metal particles was on the order of 10–20 nm. It was shown via EDS that nickel atoms predominantly agglomerated into particles, while platinum atoms were uniformly distributed over the sample. The particles were metal cores, covered partially or completely with oxide shells (Fig. 3). The EDS data and the inter-

**Table 1.** Interplanar distances on whose basis surface phases were identified

| Catalyst, wt % | Surface phase | Space group | $d$, nm | $d_1$, nm | $I$ | $N$ [14] |
|---|---|---|---|---|---|---|
| 3 Pt/C, wt % | Pt | $Fm\bar{3}m$ | 0.393 | 0.392 | 100 | 4334349 |
| | $Pt_3O_4$ | $Fm\bar{3}n$ | 0.393 | 0.395 | 011 | 1008965 |
| 0.1Pt/3Ni, wt % | $Ni_{0.92}$ $Pt_{0.08}$ | $Fm\bar{3}m$ | 0.216 | 0.216 | 111 | 1523344 |
| | NiPt | $Fm\bar{3}m$ | 0.219 | 0.219 | 111 | 1538610 |
| | | | 0.206 | 0.206 | | |
| | NiO | $C2/m$ | 0.241 | 0.240 | –111 | 1522025 |
| | | $R\bar{3}m$ | 0.209 | 0.209 | 012 | 1526380 |
| | Ni | $Fm\bar{3}m$ | 0.204 | 0.204 | 111 | 4320489 |
| | $PtO_2$ | $Pnnm$ | 0.260 | 0.258 | 110 | 1530633 |
| | $Pt_3O_4$ | $Fm\bar{3}n$ | 0.250 | 0.250 | 011 | 1008965 |
| 0.1Pt/1.5Cr, wt % | Cr | $Fm\bar{3}m$ | 0.365 | 0.368 | 100 | 1535885 |
| | $Cr_3C_2$ | $Pnma$ | 0.211 | 0.211 | 113 | 7222489 |
| | | | | 0.212 | 105 | |
| | $Pt_{3.4}O_4$ | $Fm\bar{3}n$ | 0.404 | 0.397 | 011 | 2002332 |
| 3Ni–1.5Cr, wt % | Cr | $Fm\bar{3}m$ | 0.208 | 0.208 | 111 | 1535885 |
| | $CrNi_3$ | $Fm\bar{3}$ | 0.205 | 0.205 | 111 | 1525114 |
| | $Cr_{0.4}Ni_{0.6}$ | $Fm\bar{3}m$ | 0.207 | 0.207 | 111 | 1523948 |
| | $Cr_3C_2$ | $Pnma$ | 0.210 | 0.211 | 113 | 7222489 |
| | | | | 0.212 | 105 | |
| | | | 0.224 | 0.224 | 203 | |
| | $Cr_2O_3$ | $R\bar{3}c$ | 0.264 | 0.266 | –114 | 9016327 |
| | | | 0.216 | 0.217 | –123 | |
| | $NiCrO_4$ | $Cmcm$ | 0.204 | 0.204 | 202 | 1008105 |
| | | | 0.206 | 0.206 | 040 | |
| | $NiCr_2O_4$ | $I4_1/amd$ | 0.213 | 0.213 | 042 | 1536758 |
| | | | 0.204 | 0.204 | 204 | |
| | | $Fd\bar{3}m$ | 0.208 | 0.208 | 004 | 2009226 |
| | NiO | $R\bar{3}m$ | 0.209 | 0.209 | 012 | 1526380 |
| | $Cr_3O$ | $Pm\bar{3}n$ | 0.186 | 0.186 | 112 | 1528029 |
| 0.1Pt/1.5Cr/3Ni, wt % | Cr | $Fm\bar{3}m$ | 0.214 | 0.213 | 111 | 9008467 |
| | $CrNi_3$ | $Fm\bar{3}m$ | 0.178 | 0.178 | 200 | 1525114 |
| | CrNi | $Fm\bar{3}m$ | 0.207 | 0.207 | 111 | 1525375 |
| | $Cr_{0.4}Ni_{0.6}$ | $Fm\bar{3}m$ | 0.179 | 0.179 | 200 | 1523948 |
| | | | 0.206 | 0.207 | 111 | |
| | $Cr_{23}C_6$ | $Fm\bar{3}m$ | 0.150 | 0.149 | 117 | 2107332 |
| | $Cr_3C_2$ | $Pnma$ | 0.189 | 0.188 | 044 | 7222489 |
| | | | 0.224 | 0.224 | 203 | |
| | $Pt_3O_4$ | $Fm\bar{3}n$ | 0.228 | 0.228 | 112 | 1008965 |
| | | | 0.278 | 0.279 | 002 | |
| | $PtO_2$ | $Pnnm$ | 0.224 | 0.224 | 200 | 1530633 |
| | NiO | $R\bar{3}m$ | 0.209 | 0.209 | 012 | 1526380 |
| | $NiCrO_4$ | $Cmcm$ | 0.204 | 0.204 | 202 | 1008105 |
| | | | 0.214 | 0.214 | 221 | |
| | $NiCr_2O_4$ | $I4_1/amd$ | 0.212 | 0.213 | 042 | 1536758 |
| | $NiCr_2O_4$ | $Fd\bar{3}m$ | 0.251 | 0.252 | 113 | 2009226 |

$d$, characteristic interplanar distances in the sample; $d_1$, reference values of interplanar distances; $hkl$, plane indices; $N$, card number in database.

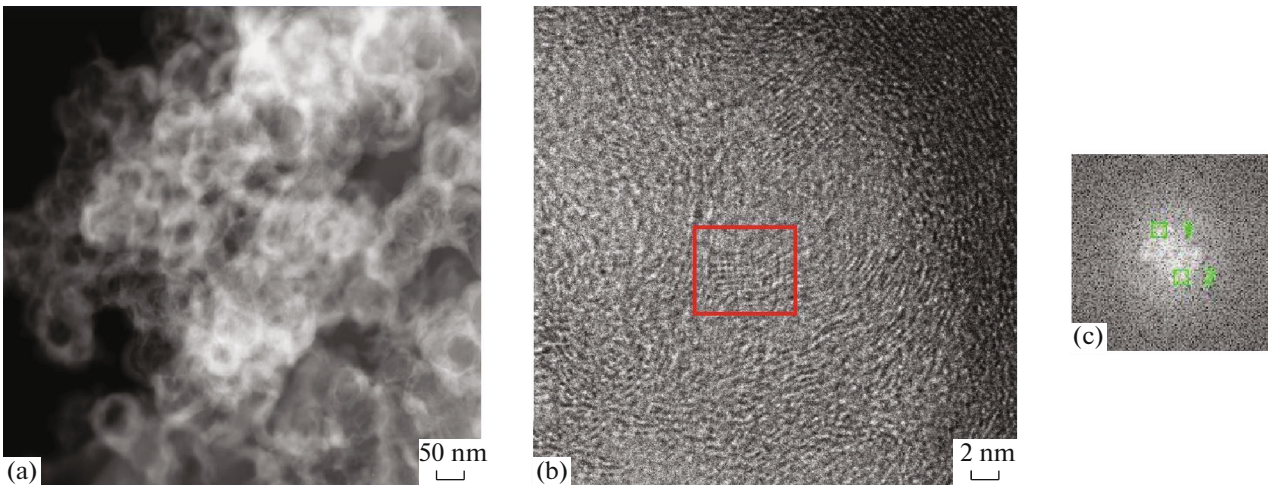


**Fig. 2.** Micrographs of the 3Pt/C surface: (a) dark field image; (b) formation of a crystalline phase; (c) selected area diffraction pattern.

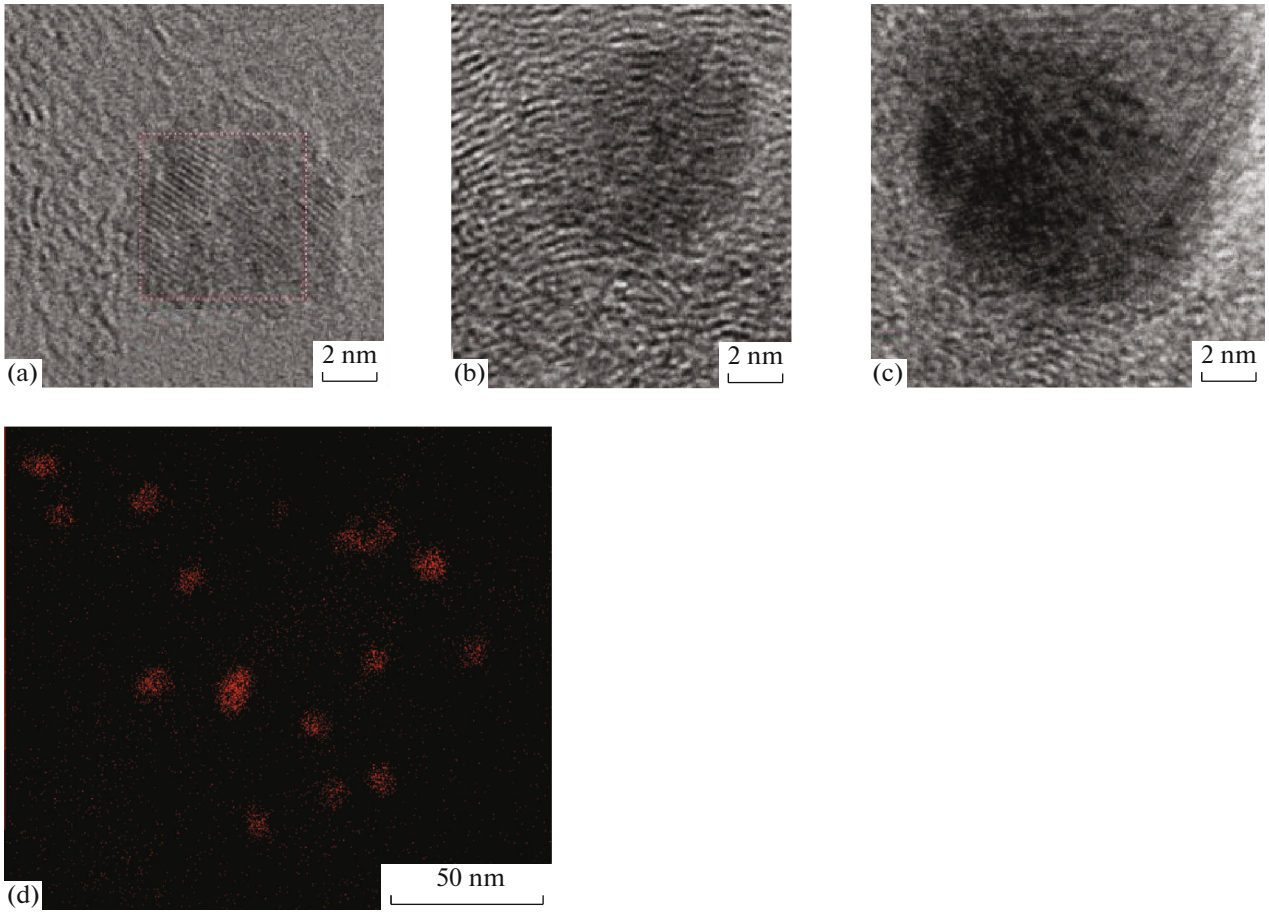


**Fig. 3.** Catalyst 0.1Pt/3Ni/C: (a–c) micrographs of metal particles, partially or completely covered with oxide shells; (d) distribution of nickel atoms on the carrier's surface.

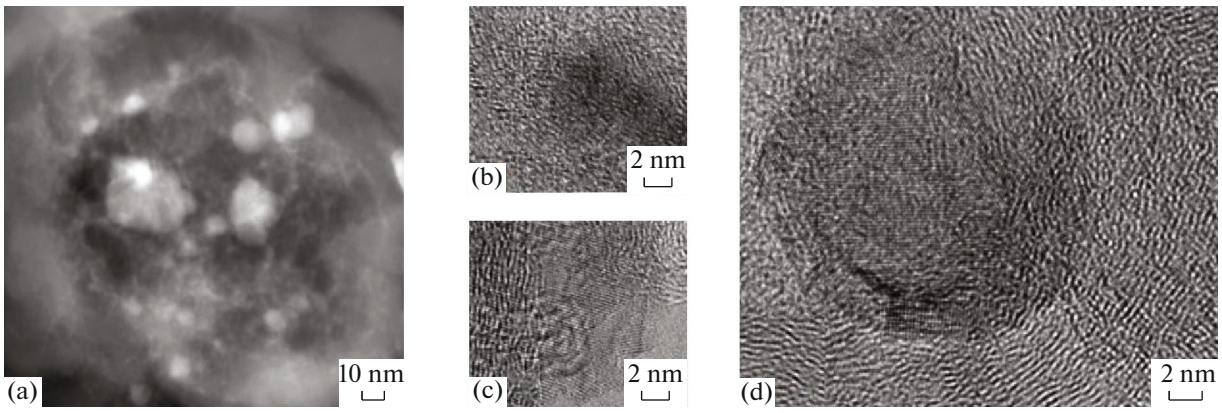


**Fig. 4.** Catalyst (3Ni–1.5Cr)/C: (a) surface phases in a dark field; (b) metallic phase; (c) carbide phase; (d) metallic/carbide phase in an oxide shell.

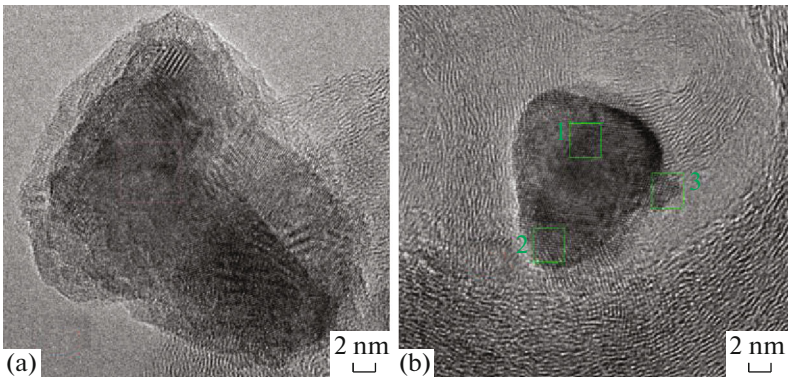


**Fig. 5.** 0.1Pt/1.5Cr/3Ni/C catalyst: (a) large catalyst particle of heterogeneous structure and composition; (b) metal particle. See text for notation.

planar distances determined from the diffraction patterns show the presence of metallic nickel and solid solutions $Pt_xNi_{1-x}$. The particle envelopes were formed by oxides NiO, $Pt_3O_4$, $PtO_2$. An unoxidized metallic phase thus appeared on the support's surface in the 0.1Pt/3Ni/C system, in contrast to the monometallic platinum catalyst.

Metal particles up to 50 nm in size form in the (3Ni–1.5Cr)/C system (Fig. 4). According to EDS data, the particles contained Ni and Cr atoms and their solid solutions $Cr_xNi_{1-x}$ in different proportions. The metal particles were covered with oxide shells, and the oxides could be identified from their interplanar distances: NiO, $Cr_2O_3$, $NiCr_2O_4$ with spinel structure and $NiCrO_4$ with a rutile structure. The formation of surface chromium carbides was also observed. Compared to the 0.1Pt/3Ni/C catalyst, the amount of metallic (unoxidized) nickel in the surface phase fell, and oxide phases predominated.

Large catalyst particles of heterogeneous structure and composition (up to 30 nm; Fig. 5a) formed in the 0.1Pt/1.5Cr/3Ni/C ternary system. The phase composition of the catalyst was close to binary systems (3Ni–1.5Cr)/C and 0.1Pt/3Ni/C: the catalyst particles were in the form of both metals (particularly in the form of substitutional solid solutions $Cr_xNi_{1-x}$, $Pt_xNi_{1-x}$) and oxides ($Pt_3O_4$, $PtO_2$, NiO, $Cr_2O_3$, $NiCr_2O_4$, $Cr_3O$). Chromium carbides ($Cr_{23}C_6$, $Cr_3C_2$) were also observed. Figure 5b shows an image of the microstructure of a metal particle with linear dimensions of the order of 15–20 nm. Diffraction patterns were obtained for individual sections of the particle, and the characteristic interplanar distances were determined. Sections *1* and *2* are metallic phases of $Cr_xNi_{1-x}$; section *3* on the surface of the metal particle contains an oxide phase.

### *Structure of Reduced Catalysts*

Figure 6 shows micrographs of the 0.1Pt/3Ni/C catalyst before and after reduction with hydrogen. Though the size distribution of metal particles is the same, the sample after reductive hydrogenation has

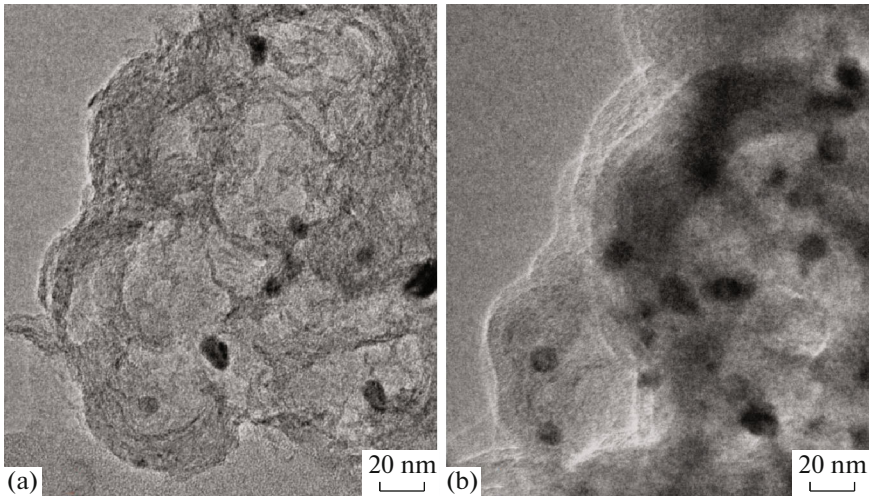


**Fig. 6.** Catalyst 0.1Pt/Ni/C (a) before and (b) after reduction with hydrogen.

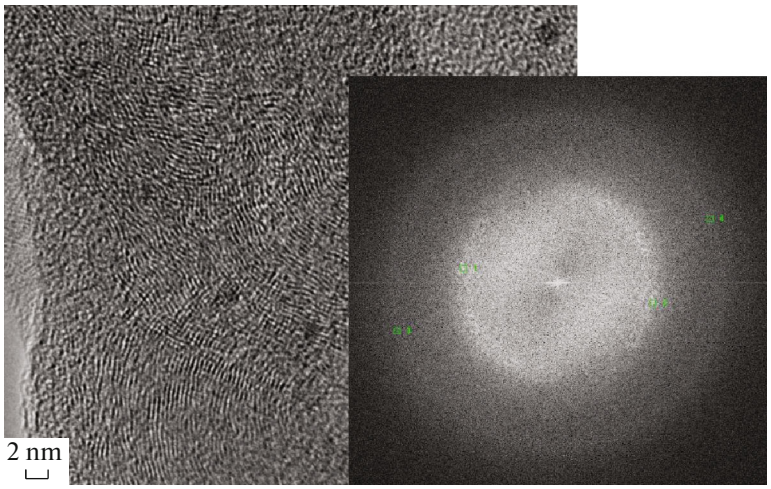


**Fig. 7.** Micrograph of the 0.1Pt/1.5Cr/C system and the diffraction pattern of the surface.

greater dispersion. Elemental analysis showed that both metals were contained in the particles.

After reduction, 0.1Pt/1.5Cr/C catalyst contained finely dispersed metal particles up to 5 nm in size. The diffraction pattern indicates the sample was amorphous (Fig. 7). The surface structure of the 0.1Pt/1.5Cr/C catalyst resembles that of the platinum catalyst (Fig. 2).

According to the EDS data, the metal particles in the 0.1Pt/(3Ni–1.5Cr)/C ternary system mainly consisted of nickel atoms. Some samples were a solid solution of $Cr_xPt_{1-x}$. In the 0.1Pt/1.5Cr/3Ni/C ternary system, which differs from the above order of depositing Cr and Ni atoms (chromium and then platinum were deposited on top of the monometallic nickel catalyst), metal particles were generally larger and also contained mainly nickel atoms (Fig. 8). The phase composition of the 0.1Pt/1.5Cr/3Ni/C catalysts before and after reduction was the same, but the particles of the reduced catalyst were more uniform in size and shape. The diffraction pattern indicates that the samples were amorphous. It should be noted that after reduction, the 0.1Pt/(3Ni–1.5Cr)/C catalyst obtained via the joint deposition of nickel and chromium salts on a support is represented more in the surface phase by chromium, metal oxides, and chromium carbides, while the surface of the metal phase of the 0.1Pt/1.5Cr/3Ni/C catalyst contained unoxidized forms of nickel and platinum after reduction.

## CONCLUSIONS

TEM was used to study the composition and structure of the surface phases of mono-, bi-, and trimetallic catalysts based on Pt, Ni, and Cr with reduced contents of the noble metal. The catalysts were deposited onto Sibunit supports and differed in the concentrations of metals and the order of their deposition (before and after reduction with hydrogen). The metal in the Pt/C system was in a highly dispersed state,

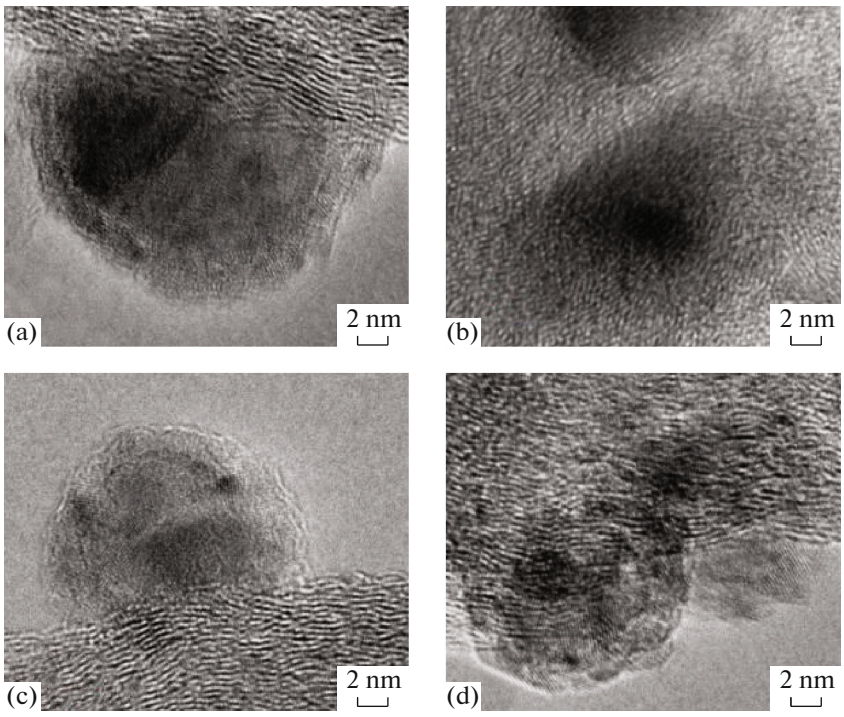


**Fig. 8.** Microstructure of catalysts 0.1Pt/1.5Cr/3Ni/C (a, b) and 0.1Pt/(3Ni–1.5Cr)/C (c, d).

mainly in an oxidized form. The surfaces of the bi- and trimetallic catalysts contained metallic and oxide components. Nickel-based catalysts were characterized by the formation of large metal particles (up to 30 nm). The surfaces of the Pt–Ni systems were characterized by an increase in the content of metallic platinum and oxidized forms of nickel. The surface of the Pt–Cr system was distinguished by high dispersion and an increase in the amount of oxidized platinum. In systems containing Ni and Cr, chromium was in reduced state, and carbides were formed along with mixed oxides of nickel and chromium. The metal phase on the surface of the Pt–Ni catalyst was more pronounced than on Ni–Cr and Pt–Ni–Cr. The components of ternary systems affect one another: in the presence of nickel, the proportion of metallic platinum increased; in the presence of chromium, metallic platinum transformed into an active oxidized state. The structure of the catalysts before and after hydrogenation were compared. Increased dispersion and reduced crystallinity of metal particles were observed each system after reductive hydrogenation.

## ACKNOWLEDGMENTS

This work was a development of the ideas of Valery Vasil'evich Lunin, Academician of the Russian Academy of Sciences, in the field of physical chemistry and heterogeneous catalysis. The authors are grateful to Prof. Lunin, a fine gentleman, scientist, and teacher.

## REFERENCES

1. L. M. Kustov, A. N. Kalenchuk, V. I. Bogdan, Russ. Chem. Rev. **89**, 897 (2020).
2. N. A. Kalenchuk, V. I. Bogdan, S. F. Dunaev, and L. M. Kustov, Fuel **280**, 118625 (2020).
3. V. I. Bogdan, A. E. Koklin, A. N. Kalenchuk, and L. M. Kustov, Mendeleev Commun. **300**, 462 (2020).
4. A. Stanislaus, and B. H. Cooper, Catal. Rev.-Sci. Eng. **36**, 75 (1994).
5. A. N. Kalenchuk, V. I. Bogdan, S. F. Dunaev, and L. Kustov, Fuel Process. Technol. **169**, 94 (2018).
6. N. Kariya, A. Fukuoka, M. Ichikawa, Appl. Catal., A **233**, 91 (2002).
7. W. Yuan, K. Scott and H. Cheng, J. Power Sources **163**, 232 (2006).
8. H. R. Colon-Mercado and B. N. Popov, J. Power Sources **155**, 253 (2006).
9. A. A. Shukla, P. V. Gosavi, J. V. Pande, et al., Int. J. Hydrogen Energy **35**, 4020 (2010).
10. A. L. Tarasov, O. P. Tkachenko, and L. M. Kustov, Catal. Lett. **148**, 1472 (2018).
11. K. Rouibah, A. Barama, R. Benrabaa, et al., Int. J. Hydrogen Energy **30**, 1 (2017).
12. P. Mani, R. Srivastava, and P. Strasser, J. Power Sources **196**, 666 (2011).
13. A. N. Kalenchuk, V. I. Bogdan, S. F. Dunaev, and L. M. Kustov, Int. J. Hydrogen Energy **43**, 6191 (2018).
14. Open Crystallographic Database. http://crystallography.net/cod/.